Published in final edited form as:
Contrast Media Mol Imaging. 2014 May ; 9(3): 221–228. doi:10.1002/cmmi.1559.

Liposome-encapsulated superoxide dismutase mimetic: theranostic potential of an MR detectable and neuroprotective agent

Mohammed Salman Shazeeb[1], **Giancarlo Feula**[2], and **Alexei Bogdanov Jr.**[1,3]

[1]Department of Radiology, University of Massachusetts Medical School, Worcester, MA 01655

[2]Worcester Polytechnic Institute, Worcester, MA 01609

[3]Cell Biology, University of Massachusetts Medical School, Worcester, MA 01655

Abstract

Endogenous manganese based superoxide dismutase (Mn-SOD) provides the primary defense against excess production of potentially toxic superoxide anion (O_2^-). M40401 is a synthetic enzyme mimetic that has a catalytic activity rate exceeding that of the native SOD enzymes. The presence of a paramagnetic Mn(II) cation in M40401 suggests that the delivery and spatial distribution of this enzyme mimetic *in vivo* may be directly detectible using magnetic resonance imaging (MRI); however, the cardiotoxicity of Mn(II) severely limits the use of free M40401 in living systems. To deliver M40401 *in vivo* in amounts sufficient for MRI detection and to limit potential cardiotoxicity, we encapsulated M40401 into 170 nm liposomes composed of phosphatidylcholine and PEGylated phosphatidylethanolamine to achieve extended circulation in the bloodstream. The obtained liposomes efficiently catalyzed superoxide dismutation *in vitro*. Using 3 T MRI we investigated the biokinetics of liposome-encapsulated M40401 in mice and found that in addition to catalyzing superoxide dismutation *in vitro*, M40401 caused differential and region-specific enhancement of mouse brain after the systemic administration. Thus, liposome encapsulated M40401 is an ideal candidate for development as a theranostic compound useful for simultaneous MRI-mediated tracking of delivery as well as for neuroprotective treatment of ischemic brain.

Keywords

liposomes; Mn-SOD; MRI; mouse brain; manganese complex; M40401

INTRODUCTION

The superoxide anion (O_2^-) is an essential component of the immune system's defense against invasion of microorganisms, but its chronic production has been shown to cause numerous deleterious effects which include the exacerbation of cardiovascular disease (1-3), and central nervous system damage following reperfusion (4-8).

The superoxide dismutase (SOD) family of enzymes (9) counteract toxicity of O_2^- by catalyzing the dismutation of O_2^- into oxygen (O_2) and hydrogen peroxide (H_2O_2), followed by the catalysis of H_2O_2 breakdown by catalase (Eqs. 1 and 2):

Correspondence: Alexei A. Bogdanov, Jr, Ph.D., Department of Radiology, University of Massachusetts Medical School, 55 Lake Avenue North, S6-326, Worcester MA 01655, Tel: 508-856-5571, FAX: 508-856-1860, Alexei.Bogdanov@umassmed.edu.

$$2O_2^- + 2H^+ \xrightarrow{SOD} H_2O_2 + O_2 \quad \text{[Eq.1]}$$

$$2H_2O_2 \xrightarrow{catalase} 2H_2O + O_2 \quad \text{[Eq.2]}$$

Mitochondrial manganese-SOD (Mn-SOD) provides the primary defense against excess production of O_2^- (10). Mn-SOD deficiency in cells has been shown to exacerbate cerebral infarction following focal cerebral ischemia in mice (11,12). Therapeutics such as Tamoxifen (13), naloxone (14), and curcumin (15) that provide neuroprotection after cerebral ischemia, appear to exert their beneficial effects in part by attenuating O_2^- production and increasing endogenous Mn-SOD. Furthermore, synthetic Mn-SOD mimetics such as water-soluble Mn-porphyrins (reviewed in (16)), salen-manganese complexes (17), and macrocyclic mimetics, e.g. M40401 (18), have been shown to protect against cerebral damage.

M40401 (Fig. 1) is an SOD mimetic with a history of *in vivo* testing whose catalytic rate exceeds 1.10^9 $[M{\cdot}s]^{-1}$, comparable to the native Cu/Zn SOD enzymes (16,19). The presence of the paramagnetic Mn(II) (Mn^{2+}) in M40401 suggests that the *in vivo* distribution and kinetics of this compound should be directly detectable by MRI, thus giving M40401 combined therapeutic and diagnostic (theranostic) potential.

Mn^{2+} has been extensively used as a T_1 contrast agent in manganese-enhanced MRI (MEMRI) studies for animal neuroimaging (20,21) and as a redox-sensitive probe (22,23). It has been proven reliable in visualizing brain neuroarchitecture (24,25). However, free Mn^{2+} cation exhibits toxicity which is partially due to the fact that it accumulates in mitochondria similar to Ca^{2+}, and cleared very slowly from the brain (26). The pronounced cardiotoxicity of free Mn^{2+} has been investigated extensively and attributed to competitive calcium antagonism due to Mn^{2+} permeation into cardiomyocytes (27,28). To circumvent the problem of toxicity, various manganese compounds can be encapsulated into liposomes and micelles which can be used for designing MR contrast agents (29-33). In the case of brain imaging, liposomes can be delivered systemically through the vasculature or directly into the brain using convection-enhanced delivery (CED) (34,35). In addition, liposomes provide longer circulation times for contrast agent delivery to organs such as liver, spleen, brain and cartilage (29,30,34-40). Studies utilizing liposomes loaded with neuroprotective agents such as SOD (41), Fasudil (42), hemoglobin (43-45), and citicoline (46), have shown a reduction in cerebral infarction in rat models of cerebral ischemia.

In this study, we tested the hypothesis that encapsulation of M40401 into long-circulating PEGylated liposomes would enable delivery of M40401 to the brain following IV injection of M40401-loaded liposomes that serve as a depot for the eventual release of the mimetic, while simultaneously negating the toxic effects of Mn^{2+}, and preserving catalytic activity of the enzyme mimetic. We also tested the capability of MRI to follow the delivery and subsequent distribution of M40401 or Mn^{2+} in neural tissue.

MATERIALS AND METHODS

Materials

(±)-*trans*-1,2-diaminocyclohexane (99%) was purchased from Sigma-Aldrich. Manganese(II) Chloride (99.998% Mn content) was purchased from Alfa Aesar. All other reagents were analytical grade and purchased from either Sigma-Aldrich or Acros Organics.

Solvents were of the highest grade available and purchased from Fisher Scientific. All reagents and solvents were used as received.

1. Synthesis of N,N'-bis-[trans-(2-amino)cyclohexyl]-1,2-diaminoethane

Racemic trans-diaminocylohexane (10.0 g, 87.6 mmol) was dissolved in anhydrous CH_2Cl_2 (150 ml) and cooled to 0° C. A solution of trityl chloride (10.1 g, 36.5 mmol) in CH_2Cl_2 (100 ml) was added drop-wise over 2 hours. The mixture was warmed to room temperature, stirred overnight, washed with water to pH below 8.0, and dried over Na_2SO_4 to yield N-(triphenylmethyl)-*trans*-diaminocyclohexane (compound **1**) as an off-white glass. Compound **1** was dissolved in MeOH (200 ml) and glyoxal (40% aq.) was added drop-wise over 15 minutes. The cloudy mixture was stirred overnight and the precipitated product was filtered and dried by lyophilization to yield N,N'-bis-[trans-(2-triphenylmethylamino) cyclohexyl]-1,2-diiminoethane as a white powder. The latter product was dissolved in anhydrous THF and $NaBH_4$ was added slowly under a blanket of Ar. The mixture was stirred at RT overnight then warmed to 40°C for 2h. The reaction was quenched with water (25 ml) and the THF was removed under reduced pressure. The aqueous slurry was partitioned between CH_2Cl_2 (200 ml) and water (100 ml) and the aqueous fraction was extracted with CH_2Cl_2 (100 ml), dried over $MgSO_4$, filtered, and concentrated to yield N,N'-bis-[trans-(2-triphenylmethylamino)cyclohexyl]-1,2-diaminoethane (compound **2**) as an off-white foam. Compound **2** was dissolved in acetone and concentrated HCl was added. The mixture was stirred for 2h and concentrated under reduced pressure. The slurry was partitioned between CH_2Cl_2 and water and the organic phase was extracted with water. The aqueous layers were combined, concentrated, and dried by lyophilization to yield N,N'-bis-[trans-(2-amino)cyclohexyl]-1,2-diaminoethane (compound **3**) as an off-white solid.

2. Synthesis of Manganese(II) dichloro [2S,21S-dimethyl-3,10,13,20,26-pentaazatetra-cyclo[20.3.1.0.0]hexacosa-1(26),22(23),24-triene]

The synthesis was performed as described in (47) with modifications. N,N'-bis-[trans-(2-amino)cyclohexyl]-1,2-diaminoethane (compound **3**) (4.38g, 10.94mmol) was dissolved in anhydrous ethanol (110ml) and flushed with Ar. KOH (2.46 g, 4 eq.) was added in one portion and the mixture was warmed to 30° C and stirred until compound **3** was dissolved, precipitating KCl. $MnCl_2$ (1.38g, 10.94mmol) was added in one portion and stirring continued for 1 h until all the $MnCl_2$ had dissolved and a color change from white to green-grey was observed. 2,6-diacetylpyridine (1.79g, 10.94mmol) was added in one portion and stirred for 30 minutes at room temperature and refluxed for 96 h. The deep-red mixture was filtered and the filtrate was concentrated to yield crude manganese bisimine macrocycle (compound **4**, 2.48g). Compound **4** was dissolved in MeOH and flushed with Ar. Pd/C (3%, 50% wet, 1.24 g) was added under Ar and the suspension was heated to 45° C. Ammonium formate (1.24 g) was added and the solution was heated to reflux. One hour after reflux, a second portion of formate was added (0.62 g) and the mixture was heated for another 2 h. The suspension was cooled and filtered and MeOH was removed under reduced pressure to yield the crude macrocycle as a red solid. A Bakerbond C_{18} (80 g, Baker) flash chromatography column was equilibrated sequentially with CH_3CN, 0.5 M NaCl/CH_3CN (1:1) followed by 18% CH_3CN in 0.25 M NaCl. The sample was dissolved in water and the pH was adjusted to 7.5. The product was eluted isocratically with 18% CH_3CN in 0.25 M NaCl. NaCl was added to the aqueous fractions containing the desired product to adjust the concentration to approximately 1 M and the fractions were extracted with CH_2Cl_2, dried over Na_2SO_4, and concentrated. The resultant compound was suspected to be a mixture of two diastereomers (compounds **5** and **6**), which were separated out by preparative reversed-phase HPLC using a gradient of 0.25 M NaCl -80% of CH_3CN/water. MS (MALDI) *m/z* = 509$[M-H]^-$, 528$[M+H_3O]^+$.

3. Liposome preparation

Liposomes containing M40401 were prepared using a mixture of distearoyl phosphatidylcholine (DSPC) and PEGylated distearoyl phosphatidyl-ethanolamine (DSPE)-PEG(2000) (90:10 mol/mol). Lipids were dissolved in chloroform and a thin lipid film was created by rotary evaporation. Water solutions of M40401 were added to the film and the lipids were hydrated for 60 min with the formation of multilamellar vesicles at 65°C. Unilamellar liposomes were formed by extruding the liposomes using Liposo-Fast (Avestin) assembly through stacked Nuclepore membranes with a 200 nm pore size at above the phase transition temperature 20 times. Unencapsulated M40401 was removed using a PD-10 Sephadex G-25 size exclusion spin-column (GE Healthcare) equilibrated with DPBS buffer, pH 6.8.

4. Liposome characterization

Quasi-elastic-light (QEL) scattering was used to determine liposome diameters and population homogeneity using Zetasizer Nano NS (Malvern Instruments Inst., Westborough, MA). Negative contrast transmission electron microscopy was performed using a Philips CM 10 instrument at 60 kV using a staining protocol described in (48).

5. Superoxide dismutase activity measurements

The activity of various concentrations of SOD (from bovine erythrocytes, 2500 U/mg, Sigma) and SOD mimetics (M40401 and M40401 liposomes) was assessed by using 0.1 mM xanthine and 20 mU/ml xanthine oxidase (from buttermilk, Sigma) to generate superoxide in a reaction buffer (0.05M Tris hydrochloride, 0.025M NaCl, 0.025M KCl, pH 7.5). A mixture of 0.2U/ml horseradish peroxidase (HRP, Sigma)/50 μM Amplex Red was used as a dismutation detection system. The formation of hydrogen peroxide (i.e. the product of dismutation of superoxide) was detected by measuring the kinetics of the formation of fluorescent resorufin product (λ_{ex} 571/λ_{em} 585 nm) in the presence of peroxidase or by measuring resorufin absorbance changes at 560 nm.

6. Animal imaging

All animal experiments were performed as approved by the Institute Animal Care and Use Committee (IACUC) of the University of Massachusetts Medical School (Worcester, MA, USA). DBA/2 female mice (NCI Frederick) (n=5), weighing 20-25 g, were injected with M40401 liposomes. The animals were then imaged using MRI. For administration of encapsulated M40401, a 29-gauge polyurethane catheter (Strategic Applications Inc.) capped with a needle port was placed in the tail vein. A respiratory sensor was placed near the chest area to monitor the respiration rate throughout the imaging session. Throughout the imaging sessions, animals were anesthetized using 1% isofluorane in an oxygen gas mixture. The mice were positioned in a 38 mm diameter, 55 mm long birdcage RF coil, the nose was covered with a nose cone for administration of anesthesia, and the head was placed in the center of the coil. A circulating water heating blanket was placed under the mouse/RF coil assembly.

7. MRI protocol

A Philips Achieva 3.0T/60 cm MRI equipped with 80mT/m actively shielded gradients was used for performing all MRI experiments. To monitor the temporal evolution of signal enhancement in the brain following M40401 liposome delivery, multi-slice, T_1-WT MR images (TR/TE/FA = 192 ms/5.5 ms/75°) were acquired using gradient-echo sequence at various time points after M40401 liposome administration. Other imaging parameters were: slice thickness = 1 mm; slice separation (center-to-center) = 1.1 mm; field-of-view (FOV) = 15 mm × 15 mm; data acquisition matrix = 256 × 256; NEX = 8. Prior to M40401 liposome

administration, pre-contrast images were acquired followed by IV injection of M40401 liposomes at an M40401 dose of 12 μmol/kg. Several T_1-WT images were then acquired sequentially every five minutes up to the first hour and then at longer time intervals upto 4 days. Imaging of *in vitro* phantom samples was done to perform relaxivity quantifications of M40401 and M40401 liposomes at 0.47 T using a spin-echo sequence with TR/TE = 200/30 ms and NEX=1. Phantoms were also imaged at 3 T using the same gradient-echo sequence used for animal imaging (TR/TE/FA/NEX = 192 ms/5.5 ms/75°/4). Saturation recovery was also performed at 3 T using a spin-echo sequence at TR intervals ranging from 100-4000 ms (TE/NEX = 8.2 ms/1) to estimate the T_1 of the phantom samples.

8. Image analysis

Following IV infusion of M40401 liposomes, the temporal evolution of the signal change in the mouse brain was evaluated separately for several regions of the brain: cerebellum, subcortex, cortex, caudate nucleus, hippocampus, olfactory bulb as well is in pituitary gland (Fig. 4). Depending on the region-of-interest (ROI), one to seven image slices were selected covering the entire ROI at each time-point. The ROI was carefully drawn around the boundary of the contrast-enhanced region for each slice using the ImageJ software package (49). The mean signal intensity value within the ROI was then calculated using ImageJ. For each animal, the ROI signal intensity data within each brain region was averaged to generate a time-series plot for each ROI. Signal-intensities acquired post contrast administration were normalized relative to pre-contrast signal intensities to correct for any variability in initial M40401 dose:

$$ROI_{\Delta} = \frac{ROI_{post} - ROI_{pre}}{ROI_{pre}} \times 100 \quad \text{[Eq.3]}$$

where ROI_{Δ} is the percent change in ROI intensity, ROI_{post} is the mean signal intensity at a time after M40401 liposome administration, and ROI_{pre} is the mean signal intensity prior to the administration of M40401 liposomes. The signal-to-noise ratio of the brain ROI (SNR_{region}) was calculated as:

$$SNR_{region} = \frac{ROI_{region}}{SD_{noise}} \quad \text{[Eq.4]}$$

where ROI_{region} is the mean signal intensity of the ROI, and SD_{noise} is the standard deviation of noise in the corresponding slice. Analysis of variance (ANOVA) for mixed models was used to determine if there was a significant change in brain signal enhancement: (1) at different time-points after M40401 liposome injection, (2) between different brain regions, and (3) due to interaction between the time after liposome injection and the different brain regions. The Tukey-Kramer HSD multiple comparisons procedure was used to determine if any significant differences existed between the groups. Statistical analyses were carried out using the SAS statistical software package (SAS Institute Inc., Cary, NC, USA).

RESULTS

Transmission electron microscopy using negative contrast demonstrated the formation of DSPC/DSPE-PEG(2000) liposomes under the conditions chosen for loading with M40401 (Fig. 2). Quasi-elastic light scattering established the diameter of the liposomes to be 170 ± 50 nm (mean ± SD). Final liposome preparation contained approximately 0.8 μmol of M40401 per milligram of lipid and the yield of M40401 encapsulation into liposome was approximately 6%. The attempts to incorporate M40401 by mixing solutions of M40401 in ethanol with lipids before preparing a lipid film did not result in improved encapsulation

yields after hydrating the film in PBS. At 0.47 T, the relaxivity of free M40401 was approximately 4.4 $[mM.s]^{-1}$ (Fig. 3A). T_1 measurements at 0.47 T showed relaxation times of 2184 ± 29 ms and 747 ± 6 ms for intact and lysed liposomes, respectively (Fig. 3B). At 3 T, intact and lysed liposomes showed T_1 relaxation times of 2981 ± 169 ms and 695 ± 33 ms, respectively, (Figs. 3C and 3D: samples 4 and 1) while T_1 of free M40401 was 176 ± 12 ms and T_1 of DPBS was 2833 ± 263 ms (Figs. 3C and 3D: samples 3 and 2). The relaxivity of M40401 at 3 T was estimated to be approximately 1.2 $[mM.s]^{-1}$, which is comparable to that of MnDPDP at the same field strength (50).

The catalysis of superoxide dismutation was studied by detecting hydrogen peroxide in the presence of a peroxidase/Amplex Red reporting system. The percent change in V_{max} (initial reaction rate) relative to background absorbance change is shown in Fig. 4 as a function of M40401 and SOD concentrations. The change in V_{max} increased steadily for SOD, M40401, and M40401 liposomes with increasing concentrations of SOD and M40401, respectively. The value of V_{max} change was similar for M40401 liposomes and SOD up to 100 μM M40401 and 20 mU/ml SOD. However, at M40401 concentrations of 150 μM and greater and SOD concentrations of 30 mU/ml and greater, both free M40401 and M40401-loaded liposomes displayed double the increase in V_{max} than SOD at the same equivalent concentrations. V_{max} change in M40401 was greater than M40401 liposomes up to 150 μM; the SOD-like activity of M40401 and M40401 liposomes were very similar at concentrations greater than 150 μM.

In mouse experiments, within minutes after M40401 liposome injection IV, signal enhancement was observed in several brain structures and in the pituitary gland (Fig. 5). During the first hour, the pituitary gland showed the greatest signal enhancement with a maximum of 50% of the pre-injection levels (Fig. 5E). The cerebellum and subcortex regions showed signal enhancements of about 20%, and the cortex, caudate nucleus, and hippocampus regions showed a 10% signal enhancement (Fig. 5D and 5E). The olfactory bulb showed the least signal enhancement at about 5% (Fig. 5E). Fig. 6 shows the signal enhancement throughout the brain of a representative animal after M40401 liposome injection IV with the subcortex region showing greater enhancement than the cortex region. The signal enhancement in all brain regions returned near the baseline by day 4. ANOVA test for mixed models showed a significant effect of M40401 liposome injection for brain region ($p<0.0001$) and time point ($p<0.01$) after liposome injection. The interaction of brain region and post-liposome injection time point did not show a statistically significant result.

DISCUSSION

Mn-SOD mimetics have previously shown promise in treating of ischemic insult in the brain due to their neuroprotective properties (18,51). Macrocyclic mimetic M40401 harbors two molecules of water in the inner coordination sphere of paramagnetic Mn (II) cation (47). Moreover, as shown by Wang and Westmoreland (52), Mn(II) complexes with lower coordination numbers exhibit higher molar longitudinal relaxivity than Mn(II) complexes with higher coordination numbers. In fact, the relaxivity of Mn complexes with coordination number 7 ranged between 3.3 and 4.7 $[mM.s]^{-1}$ which is in agreement with the relaxivity of M40401 complex at 20 MHz and 40°C measured in our study. Thus, our assumption that the SOD mimetic M40401 has a certain potential for development as a theranostic agent was supported by solid theoretical and experimental background.

Due to its concentration-dependent toxicity, M40401 cannot be bolus-injected directly into the bloodstream to afford sufficient MR contrast in the brain. Nevertheless, toxic manganese chelates (e.g. boronated radiosensitizer Mn(II) porphyrin) in the past have been successfully administered in high doses after formulating them into liposomes for systemic delivery

(33,53). In this study, we encapsulated M40401 into PEGylated liposomes and administered them in mice to investigate the uptake of M40401 in the normal brain. With M40401 liposomes, we were able to deliver twice the dose (12 μmol/kg) compared to other similar macrocyclic Mn-SOD mimetics, e.g. M40403 (6 μmol/kg), into the bloodstream (54). We assumed that M40401 liposomes would allow controlled and gradual release of amphiphilic M40401, thus reducing its toxic effects, and the interaction of the released M40401 with bulk water will shorten T_1 relaxation time of water protons. Paramagnetic metals such as gadolinium, manganese and iron have been encapsulated in liposomes and used to target liver and spleen to observe the uptake via contrast-assisted MR images (29). Manganese-based liposomes have also been used where the manganese is not simply entrapped in the liposomes but also incorporated in the membrane bilayer of the liposomes due to binding of Mn^{2+} to the headgroups of modified phospholipids and effectively used to visualize tumors (31,32).

Our initial tests showed that M40401 could be encapsulated in liposomes with reasonable yields by using a standard extrusion method. The gel-to-liquid crystalline phase-transition temperature (T_m) of the liposomal lipid bilayer in the case of DSPC (T_m=55°C (55)) and its mixtures with low amounts of PEGylated DSPC covers the entire range of physiological temperatures. In the gel state of liposome bilayer, the r1 of liposomal M40401 is reduced due to shielding of the paramagnetic centers of Mn complex from bulk water. In addition, the r1 of liposomal M40401 is exchange limited due to slow water exchange between the liposomal interior and the bulk water solvent (56). As a result, compared to lysed M40401 liposomes and free M40401, the intact M40401 liposomes showed little signal enhancement at 3 T (Fig. 3D: sample 4). Our measurements showed that T_1 relaxation times of lysed liposomes decreased 3-fold at 0.47 T and 3 T compared to intact liposomes confirming the encapsulation of M40401 within the liposomes (Fig. 3). This relaxation enhancement is attributable to both marked increase in transmembrane water permeability, yielding fast exchange conditions, and also to potential increased availability of amphiphilic Mn complex coordinated water exchange with the bulk water (57).

Since O_2^- is capable of traversing closed erythrocyte ghosts (58) and has limited ability to penetrate pure lipid bilayer (58,59) we further tested whether the obtained PEGylated liposome formulations of M40401 had SOD-like activity similar to that of free M40401 (Fig. 4). The obtained results suggest that M40401-loaded liposomes, unlike SOD encapsulated in liposomes (58), are efficient catalysts of O_2^- dismutation (Fig. 4) in their intact state. Since intact liposomes were equally efficient as free M40401, the observed effect suggests that amphiphilic M40401 is partially embedded in membranes and is available for O_2^- dismutation.

After IV injection of M40401-loaded liposomes, initial enhancement in the mouse brain was visible within minutes, and gradually decreased over the course of the next 4 days (Fig. 6). The release of M40401 from liposomes could have occurred due to one of the following factors or a combination thereof: 1) the M40401 that resided within the lipid layer diffused out into the plasma; 2) the plasma proteins caused disruption of the liposomes that led to the release of M40401 from the liposomal aqueous region; 3) a fraction of the liposomes released the M40401 due to membrane disruption at body temperature even though the T_m of the liposomes is above the body temperature. Fossheim et al. demonstrated similar release of contrast agent at temperatures well below the T_m of liposomes with liposomal Gd-DTPA-BMA (56).

The pattern of enhancement and clearance of MR T_1-weighted signal is consistent with the entry of M40401 into the vascular bed of the brain. Previous studies have shown that lipophilic Mn porphyrins are able to penetrate the blood-brain barrier (BBB) (60). Though

there is a possibility for M40401 to enter the BBB due to its amphiphilicity, the regional analysis of brain enhancement patterns (Fig. 5) suggests that M40401 enters the cerebrospinal fluid (CSF) primarily via the choroid plexus into the ventricles. The percolation of CSF in the ventricles towards the posterior and ventral region of the brain (61) results in the observed characteristic enhancement of the cerebellum and subcortex regions. The proximity of these regions to the ventricles in the line of CSF flow can explain the constant influx of M40401. The pituitary gland showed the highest enhancement which was equivalent to that of the vasculature, consistent with its location outside of the BBB. The other regions, i.e. cortex, hippocampus, and caudate nucleus, though within the vicinity of the ventricles, showed lower enhancement immediately after injection presumably because the CSF in the ventricles flows away from the direction of these regions thereby causing slower uptake of M40401. The olfactory bulb, being the most distal region of the regions analyzed, showed the least overall enhancement. Clearance of contrast by the fourth day from most of the regions suggests that the liposomes were cleared from the circulation eventually by the mononuclear phagocyte system (62).

CONCLUSION

We established that M40401 is a highly efficient SOD mimetic that doubles as a paramagnetic contrast agent, thus being one of the few truly theranostic compounds useful for MR imaging. Liposomes loaded with paramagnetic M40401 resulted in transient enhancement of several regions of the mouse brain. To the best of our knowledge, this is the first such MRI study showing brain uptake of an Mn-SOD mimetic. Our results indicate that M40401 liposomes enable systemic delivery of an SOD mimetic to the brain that can potentially counteract high and damaging levels of O_2^- produced during cerebral ischemia while allowing MRI monitoring of therapeutic delivery to the diseased tissues.

Acknowledgments

This work was supported by 5RO1AG034901-03 and 5R01EB000858 grants to AB. We are grateful to Jamie O'Callaghan, Dr. Suresh Gupta, and Dr. Shaokuan Zheng for assistance with several technical aspects of this work. We are grateful to Dr. Mary Mazzanti for editing the text.

REFERENCES

1. Kerr S, Brosnan MJ, McIntyre M, Reid JL, Dominiczak AF, Hamilton CA. Superoxide anion production is increased in a model of genetic hypertension: role of the endothelium. Hypertension. 1999; 33(6):1353–1358. [PubMed: 10373215]
2. Miller FJ Jr. Gutterman DD, Rios CD, Heistad DD, Davidson BL. Superoxide production in vascular smooth muscle contributes to oxidative stress and impaired relaxation in atherosclerosis. Circ Res. 1998; 82(12):1298–1305. [PubMed: 9648726]
3. Mugge A, Brandes RP, Boger RH, Dwenger A, Bode-Boger S, Kienke S, Frolich JC, Lichtlen PR. Vascular release of superoxide radicals is enhanced in hypercholesterolemic rabbits. J Cardiovasc Pharmacol. 1994; 24(6):994–998. [PubMed: 7898085]
4. Kondo T, Reaume AG, Huang TT, Carlson E, Murakami K, Chen SF, Hoffman EK, Scott RW, Epstein CJ, Chan PH. Reduction of CuZn-superoxide dismutase activity exacerbates neuronal cell injury and edema formation after transient focal cerebral ischemia. J Neurosci. 1997; 17(11):4180–4189. [PubMed: 9151735]
5. Forman LJ, Liu P, Nagele RG, Yin K, Wong PY. Augmentation of nitric oxide, superoxide, and peroxynitrite production during cerebral ischemia and reperfusion in the rat. Neurochem Res. 1998; 23(2):141–148. [PubMed: 9475507]
6. Kim CD, Shin HK, Lee HS, Lee JH, Lee TH, Hong KW. Gene transfer of Cu/Zn SOD to cerebral vessels prevents FPI-induced CBF autoregulatory dysfunction. Am J Physiol Heart Circ Physiol. 2002; 282(5):H1836–1842. [PubMed: 11959650]

7. Chan PH. Oxygen radicals in focal cerebral ischemia. Brain Pathol. 1994; 4(1):59–65. [PubMed: 8025703]
8. Patel M, Day BJ, Crapo JD, Fridovich I, McNamara JO. Requirement for superoxide in excitotoxic cell death. Neuron. 1996; 16(2):345–355. [PubMed: 8789949]
9. Jung JE, Kim GS, Chen H, Maier CM, Narasimhan P, Song YS, Niizuma K, Katsu M, Okami N, Yoshioka H, Sakata H, Goeders CE, Chan PH. Reperfusion and neurovascular dysfunction in stroke: from basic mechanisms to potential strategies for neuroprotection. Mol Neurobiol. 2010; 41(2-3):172–179. [PubMed: 20157789]
10. Chan PH. Role of oxidants in ischemic brain damage. Stroke. 1996; 27(6):1124–1129. [PubMed: 8650725]
11. Murakami K, Kondo T, Kawase M, Li Y, Sato S, Chen SF, Chan PH. Mitochondrial susceptibility to oxidative stress exacerbates cerebral infarction that follows permanent focal cerebral ischemia in mutant mice with manganese superoxide dismutase deficiency. J Neurosci. 1998; 18(1):205–213. [PubMed: 9412501]
12. Kim GW, Kondo T, Noshita N, Chan PH. Manganese superoxide dismutase deficiency exacerbates cerebral infarction after focal cerebral ischemia/reperfusion in mice: implications for the production and role of superoxide radicals. Stroke. 2002; 33(3):809–815. [PubMed: 11872908]
13. Wakade C, Khan MM, De Sevilla LM, Zhang QG, Mahesh VB, Brann DW. Tamoxifen neuroprotection in cerebral ischemia involves attenuation of kinase activation and superoxide production and potentiation of mitochondrial superoxide dismutase. Endocrinology. 2008; 149(1): 367–379. [PubMed: 17901229]
14. Chen CJ, Cheng FC, Liao SL, Chen WY, Lin NN, Kuo JS. Effects of naloxone on lactate, pyruvate metabolism and antioxidant enzyme activity in rat cerebral ischemia/reperfusion. Neurosci Lett. 2000; 287(2):113–116. [PubMed: 10854725]
15. Sumanont Y, Murakami Y, Tohda M, Vajragupta O, Watanabe H, Matsumoto K. Prevention of kainic acid-induced changes in nitric oxide level and neuronal cell damage in the rat hippocampus by manganese complexes of curcumin and diacetylcurcumin. Life Sci. 2006; 78(16):1884–1891. [PubMed: 16266725]
16. Miriyala S, Spasojevic I, Tovmasyan A, Salvemini D, Vujaskovic Z, St Clair D, Batinic-Haberle I. Manganese superoxide dismutase, MnSOD and its mimics. Biochim Biophys Acta. 2012; 1822(5): 794–814. [PubMed: 22198225]
17. Baker K, Marcus CB, Huffman K, Kruk H, Malfroy B, Doctrow SR. Synthetic combined superoxide dismutase/catalase mimetics are protective as a delayed treatment in a rat stroke model: a key role for reactive oxygen species in ischemic brain injury. J Pharmacol Exp Ther. 1998; 284(1):215–221. [PubMed: 9435181]
18. Shimizu K, Rajapakse N, Horiguchi T, Payne RM, Busija DW. Protective effect of a new nonpeptidyl mimetic of SOD, M40401, against focal cerebral ischemia in the rat. Brain Res. 2003; 963(1-2):8–14. [PubMed: 12560107]
19. Cuzzocrea S, Mazzon E, Dugo L, Caputi AP, Aston K, Riley DP, Salvemini D. Protective effects of a new stable, highly active SOD mimetic, M40401 in splanchnic artery occlusion and reperfusion. Br J Pharmacol. 2001; 132(1):19–29. [PubMed: 11156557]
20. Lin YJ, Koretsky AP. Manganese ion enhances T1-weighted MRI during brain activation: an approach to direct imaging of brain function. Magn Reson Med. 1997; 38(3):378–388. [PubMed: 9339438]
21. Pautler RG, Silva AC, Koretsky AP. In vivo neuronal tract tracing using manganese- enhanced magnetic resonance imaging. Magn Reson Med. 1998; 40(5):740–748. [PubMed: 9797158]
22. Aime S, Botta M, Gianolio E, Terreno E. A p(O(2))-Responsive MRI Contrast Agent Based on the Redox Switch of Manganese(II / III) - Porphyrin Complexes. Angew Chem Int Ed Engl. 2000; 39(4):747–750. [PubMed: 10760856]
23. Chen Y, Yin Q, Ji X, Zhang S, Chen H, Zheng Y, Sun Y, Qu H, Wang Z, Li Y, Wang X, Zhang K, Zhang L, Shi J. Manganese oxide-based multifunctionalized mesoporous silica nanoparticles for pH-responsive MRI, ultrasonography and circumvention of MDR in cancer cells. Biomaterials. 2012; 33(29):7126–7137. [PubMed: 22789722]

24. Aoki I, Wu YJ, Silva AC, Lynch RM, Koretsky AP. In vivo detection of neuroarchitecture in the rodent brain using manganese-enhanced MRI. Neuroimage. 2004; 3122(2)(3):600–8. 1046–1059.
25. Koretsky AP, Silva AC. Manganese-enhanced magnetic resonance imaging (MEMRI). NMR Biomed. 2004; 17(8):527–531. [PubMed: 15617051]
26. Shazeeb MS, Sotak CH. Dose dependence and temporal evolution of the T(1) relaxation time and MRI contrast in the rat brain after subcutaneous injection of manganese chloride. Magn Reson Med. 2012
27. Wolf GL, Baum L. Cardiovascular toxicity and tissue proton T1 response to manganese injection in the dog and rabbit. AJR Am J Roentgenol. 1983; 141(1):193–197. [PubMed: 6305179]
28. Vander Elst L, Colet JM, Muller RN. Spectroscopic and metabolic effects of MnCl2 and MnDPDP on the isolated and perfused rat heart. Invest Radiol. 1997; 32(10):581–588. [PubMed: 9342116]
29. Schwendener RA, Wuthrich R, Duewell S, Wehrli E, von Schulthess GK. A pharmacokinetic and MRI study of unilamellar gadolinium-, manganese-, and iron- DTPA-stearate liposomes as organ-specific contrast agents. Invest Radiol. 1990; 25(8):922–932. [PubMed: 2394576]
30. Niesman MR, Bacic GG, Wright SM, Swartz HJ, Magin RL. Liposome encapsulated MnCl2 as a liver specific contrast agent for magnetic resonance imaging. Invest Radiol. 1990; 25(5):545–551. [PubMed: 2345086]
31. Unger E, Fritz T, Shen DK, Wu G. Manganese-based liposomes. Comparative approaches. Invest Radiol. 1993; 28(10):933–938. [PubMed: 8262748]
32. Unger E, Shen D, Fritz T, Wu GL, Kulik B, New T, Matsunaga T, Ramaswami R. Liposomes bearing membrane-bound complexes of manganese as magnetic resonance contrast agents. Invest Radiol. 1994; 29(Suppl 2):S168–169. [PubMed: 7928219]
33. Huang LR, Straubinger RM, Kahl SB, Koo MS, Alletto JJ, Mazurchuk R, Chau RI, Thamer SL, Fiel RJ. Boronated metalloporphyrins: a novel approach to the diagnosis and treatment of cancer using contrast-enhanced MR imaging and neutron capture therapy. J Magn Reson Imaging. 1993; 3(2):351–356. [PubMed: 8448397]
34. Mamot C, Nguyen JB, Pourdehnad M, Hadaczek P, Saito R, Bringas JR, Drummond DC, Hong K, Kirpotin DB, McKnight T, Berger MS, Park JW, Bankiewicz KS. Extensive distribution of liposomes in rodent brains and brain tumors following convection-enhanced delivery. J Neurooncol. 2004; 68(1):1–9. [PubMed: 15174514]
35. Saito R, Bringas JR, McKnight TR, Wendland MF, Mamot C, Drummond DC, Kirpotin DB, Park JW, Berger MS, Bankiewicz KS. Distribution of liposomes into brain and rat brain tumor models by convection-enhanced delivery monitored with magnetic resonance imaging. Cancer Res. 2004; 64(7):2572–2579. [PubMed: 15059914]
36. Unger E, Shen DK, Wu GL, Fritz T. Liposomes as MR contrast agents: pros and cons. Magn Reson Med. 1991; 22(2):304–308. discussion 313. [PubMed: 1812361]
37. Unger EC, Shen DK, Fritz TA. Status of liposomes as MR contrast agents. J Magn Reson Imaging. 1993; 3(1):195–198. [PubMed: 8428087]
38. Unger EC, Ugurbil K, Latchaw RE. Contrast agents for cerebral perfusion MR imaging. J Magn Reson Imaging. 1994; 4(3):235–242. [PubMed: 8061420]
39. Grunder W, Biesold M, Wagner M, Werner A. Improved nuclear magnetic resonance microscopic visualization of joint cartilage using liposome entrapped contrast agents. Invest Radiol. 1998; 33(4):193–202. [PubMed: 9556743]
40. Saito R, Krauze MT, Bringas JR, Noble C, McKnight TR, Jackson P, Wendland MF, Mamot C, Drummond DC, Kirpotin DB, Hong K, Berger MS, Park JW, Bankiewicz KS. Gadolinium-loaded liposomes allow for real-time magnetic resonance imaging of convection-enhanced delivery in the primate brain. Exp Neurol. 2005; 196(2):381–389. [PubMed: 16197944]
41. Imaizumi S, Woolworth V, Fishman RA, Chan PH. Liposome-entrapped superoxide dismutase reduces cerebral infarction in cerebral ischemia in rats. Stroke. 1990; 21(9):1312–1317. [PubMed: 2396268]
42. Takanashi Y, Ishida T, Kirchmeier MJ, Shuaib A, Allen TM. Neuroprotection by intrathecal application of liposome-entrapped fasudil in a rat model of ischemia. Neurol Med Chir (Tokyo). 2001; 41(3):107–113. discussion 113-104. [PubMed: 11372552]

43. Kakehata J, Yamaguchi T, Togashi H, Sakuma I, Otani H, Morimoto Y, Yoshioka M. Therapeutic potentials of an artificial oxygen-carrier, liposome-encapsulated hemoglobin, for ischemia/reperfusion-induced cerebral dysfunction in rats. J Pharmacol Sci. 2010; 114(2):189–197. [PubMed: 20838027]
44. Fukumoto D, Kawaguchi AT, Haida M, Yamano M, Ogata Y, Tsukada H. Liposome- encapsulated hemoglobin reduces the size of cerebral infarction in rats: effect of oxygen affinity. Artif Organs. 2009; 33(2):159–163. [PubMed: 19178461]
45. Kawaguchi AT, Haida M, Yamano M, Fukumoto D, Ogata Y, Tsukada H. Liposome- encapsulated hemoglobin ameliorates ischemic stroke in nonhuman primates: an acute study. J Pharmacol Exp Ther. 2010; 332(2):429–436. [PubMed: 19910538]
46. Ramos-Cabrer P, Agulla J, Argibay B, Perez-Mato M, Castillo J. Serial MRI study of the enhanced therapeutic effects of liposome-encapsulated citicoline in cerebral ischemia. Int J Pharm. 2011; 405(1-2):228–233. [PubMed: 21168478]
47. Aston K, Rath N, Naik A, Slomczynska U, Schall OF, Riley DP. Computer-aided design (CAD) of Mn(II) complexes: superoxide dismutase mimetics with catalytic activity exceeding the native enzyme. Inorg Chem. 2001; 40(8):1779–1789. [PubMed: 11312732]
48. Hendricks, G. Protocol 14: Negative Staining of AAV vector samples for high- resolution electron microscopy. In: Gao, G.; Sena-Esteves, M., editors. Molecular Cloning. Vol. 3. CSH Press; Cold Spring Harbor: 2011. p. 2-126.
49. Rasband, W. Image J. Bethesda, Maryland, USA: 1997.
50. Rohrer M, Bauer H, Mintorovitch J, Requardt M, Weinmann HJ. Comparison of magnetic properties of MRI contrast media solutions at different magnetic field strengths. Invest Radiol. 2005; 40(11):715–724. [PubMed: 16230904]
51. Mackensen GB, Patel M, Sheng H, Calvi CL, Batinic-Haberle I, Day BJ, Liang LP, Fridovich I, Crapo JD, Pearlstein RD, Warner DS. Neuroprotection from delayed postischemic administration of a metalloporphyrin catalytic antioxidant. J Neurosci. 2001; 21(13):4582–4592. [PubMed: 11425886]
52. Wang S, Westmoreland TD. Correlation of relaxivity with coordination number in six-, seven-, and eight-coordinate Mn(II) complexes of pendant-arm cyclen derivatives. Inorg Chem. 2009; 48(2): 719–727. [PubMed: 19072697]
53. Zhou R, Balasubramanian SV, Kahl SB, Straubinger RM. Biopharmaceutics of boronated radiosensitizers: liposomal formulation of MnBOPP (manganese chelate of 2,4-(alpha, beta-dihydroxyethyl) deuterioporphyrin IX) and comparative toxicity in mice. J Pharm Sci. 1999; 88(9):912–917. [PubMed: 10479353]
54. Wang ZQ, Porreca F, Cuzzocrea S, Galen K, Lightfoot R, Masini E, Muscoli C, Mollace V, Ndengele M, Ischiropoulos H, Salvemini D. A newly identified role for superoxide in inflammatory pain. J Pharmacol Exp Ther. 2004; 309(3):869–878. [PubMed: 14988418]
55. Lentz BR, Barenholz Y, Thompson TE. Fluorescence depolarization studies of phase transitions and fluidity in phospholipid bilayers. Two-component phosphatidylcholine liposomes. Biochemistry. 1976; 15(20):4529–4537. [PubMed: 974074]
56. Fossheim SL, Il'yasov KA, Hennig J, Bjornerud A. Thermosensitive paramagnetic liposomes for temperature control during MR imaging-guided hyperthermia: in vitro feasibility studies. Acad Radiol. 2000; 7(12):1107–1115. [PubMed: 11131055]
57. Aime S, Castelli DD, Crich SG, Gianolio E, Terreno E. Pushing the sensitivity envelope of lanthanide-based magnetic resonance imaging (MRI) contrast agents for molecular imaging applications. Acc Chem Res. 2009; 42(7):822–831. [PubMed: 19534516]
58. Mao GD, Poznansky MJ. Electron spin resonance study on the permeability of superoxide radicals in lipid bilayers and biological membranes. FEBS Lett. 1992; 305(3):233–236. [PubMed: 1338594]
59. Gus'kova RA, Ivanov II, Kol'tover VK, Akhobadze VV, Rubin AB. Permeability of bilayer lipid membranes for superoxide (O2-.) radicals. Biochim Biophys Acta. 1984; 778(3):579–585. [PubMed: 6095912]
60. Sheng H, Spasojevic I, Tse HM, Jung JY, Hong J, Zhang Z, Piganelli JD, Batinic-Haberle I, Warner DS. Neuroprotective efficacy from a lipophilic redox-modulating Mn(III) N-

Hexylpyridylporphyrin, MnTnHex-2-PyP: rodent models of ischemic stroke and subarachnoid hemorrhage. J Pharmacol Exp Ther. 2011; 338(3):906–916. [PubMed: 21652782]

61. Johanson CE, Duncan JA, Stopa EG, Baird A. Enhanced prospects for drug delivery and brain targeting by the choroid plexus-CSF route. Pharm Res. 2005; 22(7):1011–1037. [PubMed: 16028003]
62. Ishida T, Kashima S, Kiwada H. The contribution of phagocytic activity of liver macrophages to the accelerated blood clearance (ABC) phenomenon of PEGylated liposomes in rats. J Control Release. 2008; 126(2):162–165. [PubMed: 18160170]
63. Franklin, K.; Paxinos, G. The mouse brain in stereotaxic coordinates. Academic Press; San Diego: 1997.

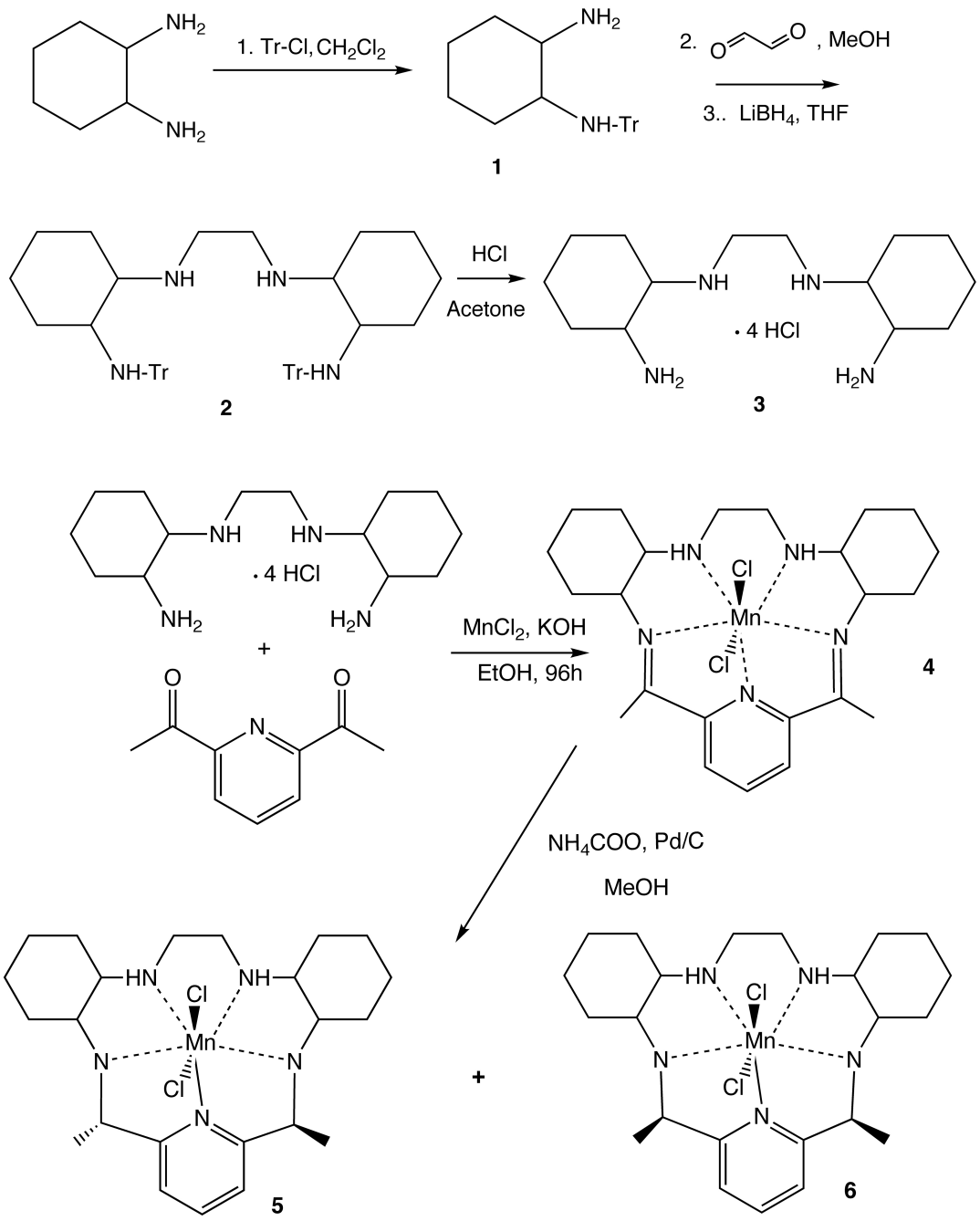

Fig. 1.

Synthesis of manganese-based superoxide dismutase mimetic, M40401 Manganese(II) dichloro [2S,21S-dimethyl-3,10,13,20,26-pentaazatetracyclo[20.3.1.0.^{4,9}0^{14,19}] hexacosa-1(26),22(23),24-triene] (compound **5**), ref. (47).

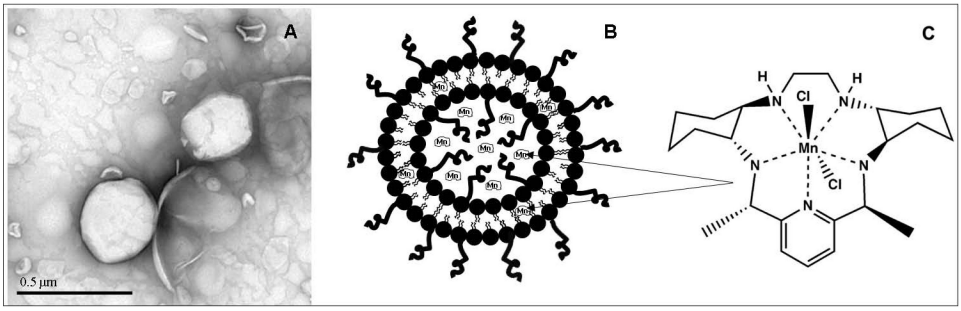

Fig. 2.

(**A**) Transmission electron micrograph of DSPC/DSPE-PEG liposomes loaded with M40401 (magnification ×25,000). (**B**) Schematic of DSPC/DSPE-PEG liposomes with M40401 in the aqueous layer. (**C**) Chemical formula of M40401 Mn complex.

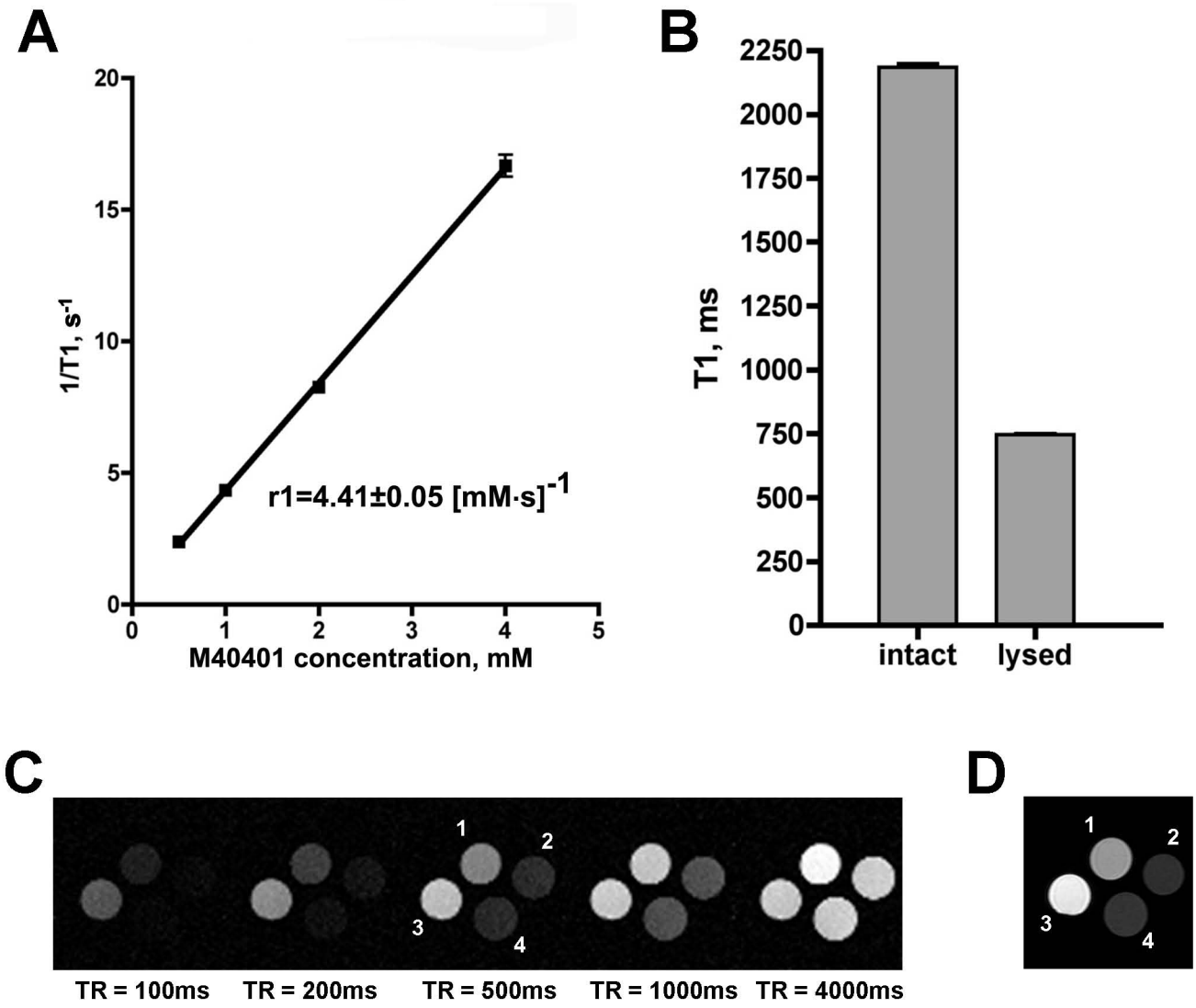

Fig. 3.

(**A**) Relaxivity of M40401 in DPBS at 0.47 T, r1 = 4.41 ± 0.05 $[mM.s]^{-1}$. (**B**) Longitudinal T_1 relaxation time of intact and lysed M40401 liposomes at 0.47 T. (**C**) 3 T saturation recovery images of four phantoms (**1**, M40401 liposomes plus detergent; **2**, DPBS solution; **3**, free M40401; **4**, M40401 liposomes in DPBS solution) using spin-echo sequence at different repetition times (TR) and TE/NEX = 8.2 ms 1 1. The T_1 values of each phantom are: **1**, 695 ± 33 ms; **2**, 2833 ± 263 ms; **3**, 176 ± 12; **4** , 2981± 169. (**D**) T_1-weighted image of the four phantoms shown in (C) at 3 T using gradient-echo sequence (TR/TE/FA/NEX = 192 ms/5.5ms/75°/4).

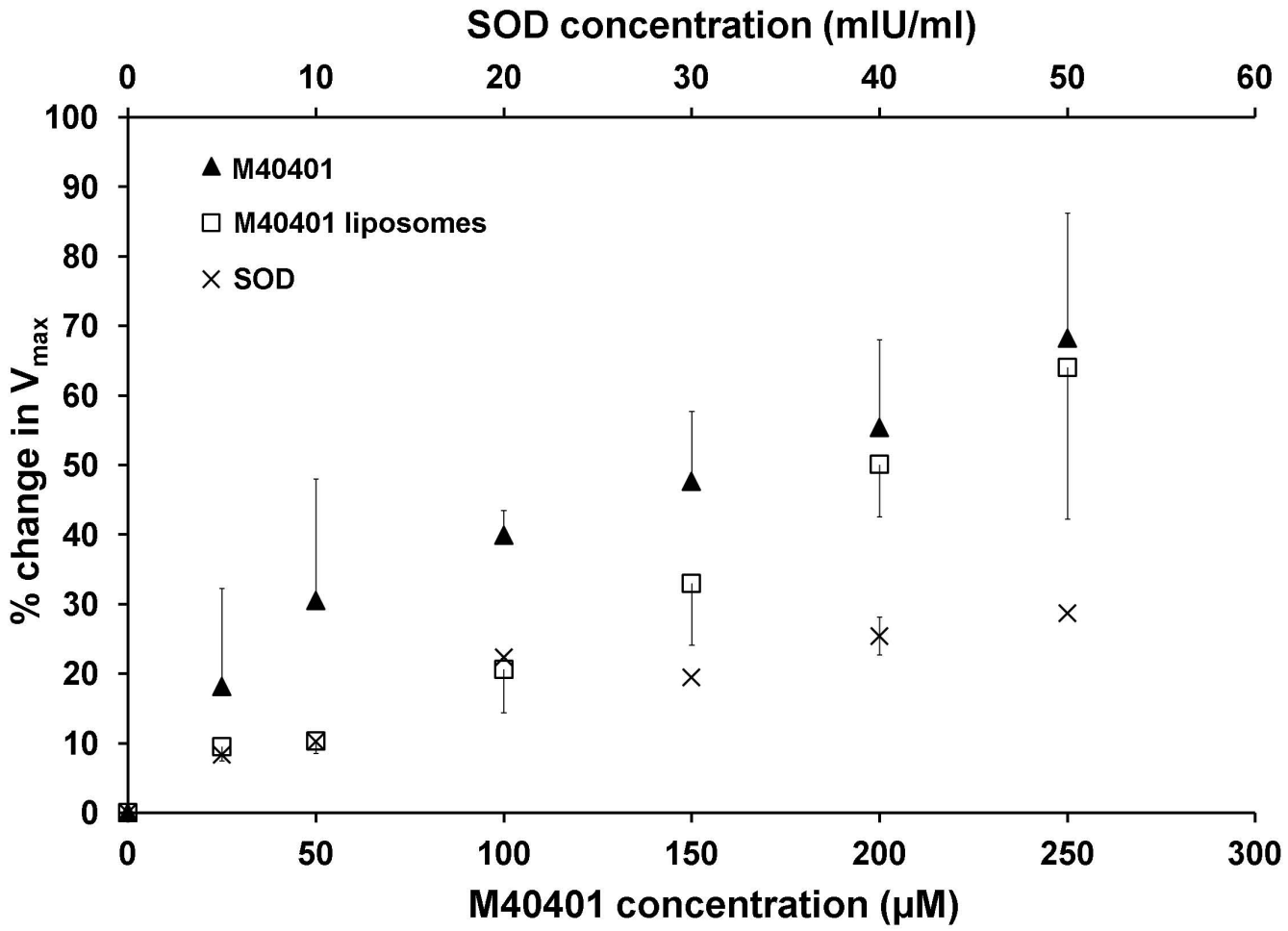

Fig. 4.

The V_{max} of superoxide dismutation measured as a function of M40401 and SOD concentrations. The reaction kinetics were measured as an increase of resorufin absorbance generated from Amplex Red in the presence of peroxidase and superoxide generating system (xanthine/xanthine oxidase). Data is represented (n=2) as mean+SD (▲), mean–SD (□), and mean±SD (×).

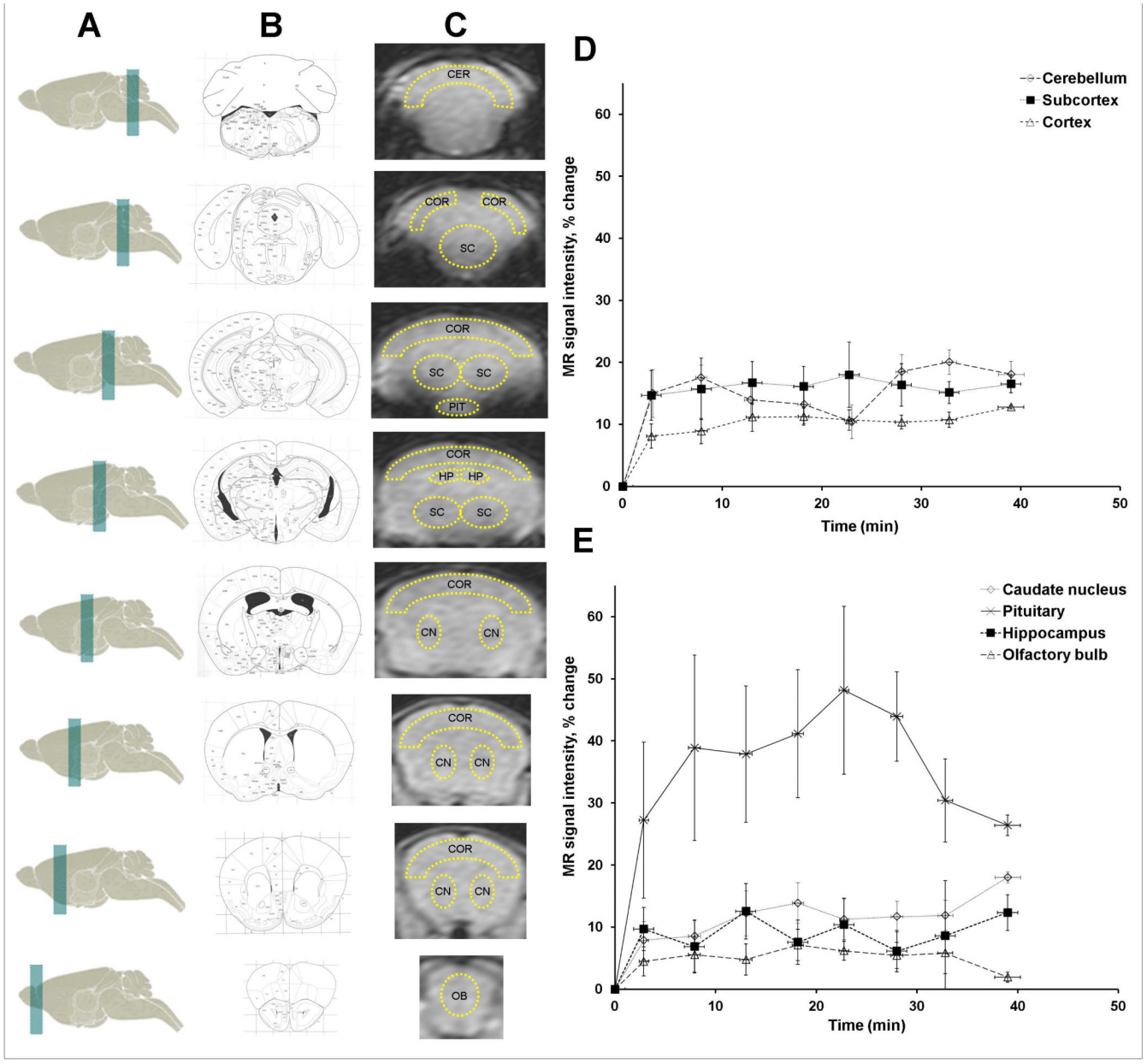

Fig. 5.

ROI definitions for different brain regions and the pituitary gland. Normalized T_1-WT signal intensities were measured in different regions of the mouse brain (n=5) after the I.V. injection of M40401 liposomes (12 μmol M40401/kg). Representative axial slices from T_1-weighted image of a mouse brain prior to liposome injection are shown (**C**) corresponding to the shaded region in the coronal slices (**A**) which correlate with schematic brain slices (**B**) from the mouse brain atlas (63). The schematic brain slices approximately correspond to the central region of the 1-mm-thick MR image slices. The different ROI regions are: CER – cerebellum; COR – cortex; SC – subcortex; CN – caudate nucleus; HP – hippocampus; PIT – pituitary gland; OB – olfactory bulb. Panels (**D**) and (**E**) show change in signal intensities normalized as percent change relative to the pre-contrast image in the different ROI regions. The graphs show the change in MR signal intensity up to approximately 40 minutes. Data are represented on both axes as mean±SEM. ANOVA test for mixed models showed a

significant effect of M40401 liposome injection on the seven different brain regions ($p<0.0001$) and time points after liposome injection ($p<0.01$).

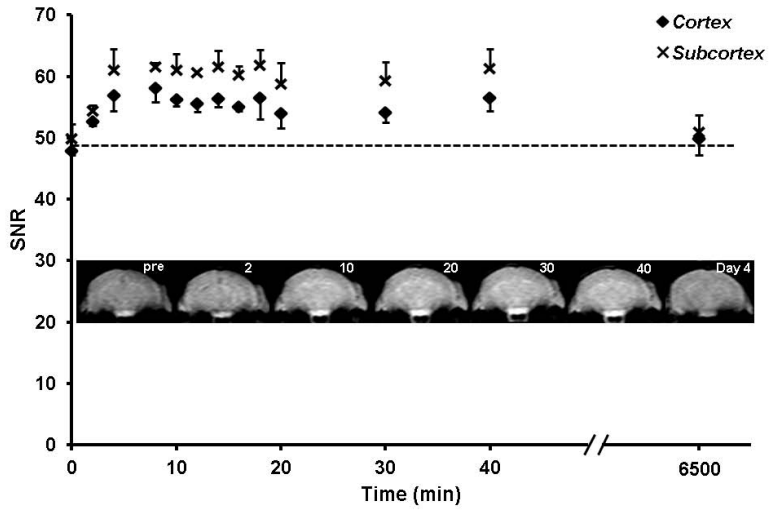

Fig. 6.

MR signal enhancement in the mouse brain with SNR as a function of time after IV injection of M40401 liposomes. The inset shows T_1-WT mouse brain images corresponding to the signal intensity curve (time in minutes). Data is shown from a representative animal across several slices in the cortex and subcortex regions as mean–SD (◆) and mean+SD (×), respectively.